scientific reports

Check for updates

OPEN

Influence of Li concentration on structural, morphological and electrochemical properties of anatase-TiO_2 nanoparticles

Thanin Putjuso[1], Sasitorn Putjuso[1], Attaphol Karaphun[2] & Ekaphan Swatsitang[2,3]✉

Lithium-doped anatase-TiO_2 nanoparticles ($Li_xTi_{1-x}O_2$ NPs, x = 0, 0.05, 0.10, 0.15 and 0.20) could be synthesized by a simple sol–gel process. X-ray diffraction (XRD) results displayed the tetragonal (space group: I41/amd) of polycrystalline TiO_2 anatase phase. The spectroscopy results of Raman and FT-IR confirmed the anatase phase of TiO_2 through the specific modes of metal oxides vibration in the crystalline TiO_2. Surfaces micrographs by scanning electron microscope (SEM) of agglomerated $Li_xTi_{1-x}O_2$ NPs showed a spongy like morphology. Transmission electron microscope (TEM) illustrated a cuboidal shape of dispersed NPs with particle size distributed in a narrow range 5–10 nm. Bruanauer Emmett-Teller (BET) results showed the increased surface area of $Li_xTi_{1-x}O_2$ NPs with increasing Li content. $Li_xTi_{1-x}O_2$ NPs (x = 0.05–0.20) working electrodes illustrated a pseudocapacitive behavior with excellent electrochemical properties through the whole cycles of GCD test. Interestingly, $Li_{0.1}Ti_{0.9}O_2$ NPs electrode illustrated a high performance in terms of maximum specific capacitance 822 F g^{-1} at 1.5 A g^{-1} in 0.5 M Li_2SO_4 electrolyte, with excellent capacitive retention 92.6% after 5000 cycles GCD test.

Keywords Lithium-doped anatase TiO_2 nanoparticles, Sol–gel method, Electrochemical properties, Supercapacitor electrodes

Supercapacitor (SC) has been demonstrated to be a beneficial gadget for advance energy storage device for present and forthcoming technology, because it can work superior than conventional capacitors in criteria of stability, capacity, and energy density. Indeed, the performance of SC device is significantly governed by the electrochemical properties of electrodes, which depend strongly on the electrode materials. In general, as suggested and reported by numerous research articles, the efficient electrode should have a huge surface area, high porosity with appropriate pore size distribution and coated on a high conducting substrate[1–4]. In some kind of SC, the chemical surface of electrode, directly correlate to the oxidation state of the materials, is considered to be an important factor that influence the electrochemical properties, as well. In addition, distinct electrodes morphology obtained by different synthesis conditions and processes can also affect the electrochemical properties of SC. However, when benchmark to battery, SC has some disadvantages of low energy density and output voltage instability. Therefore, much efforts have been driven to overcome these problems to push SC to be properly applied as a novel energy storage device in a wide scale[1–4].

Currently, TiO_2 nanoparticles (NPs) was deliberated as an excellently potential metal oxide to be applied for SCs electrode owing to its proper pseudocapacitive behavior, easy to synthesis, nontoxic, low cost and ecological friendliness[4–7]. However, TiO_2 NPs generally show low electrical conductivity, which can block their performance and needed to be improved. So far, applications of TiO_2 NPs doped with metal ions (Cu, Co, Ni, Li, Ag) have been widely investigated[4,8], because lithium (Li) is considered to be one of the most promising elements for use as a dopant. It has been applied in a number of disciplines, including passivation layers in perovskite solar cells, lithium-ion batteries, and nanosensors[9]. Li is also in charge of transporting to TiO_2 NPs and ejecting electrons. Furthermore, lithium ions are very mobile, and can be doped with TiO_2 to improve the conductivity and to improve electron transmission when oxygen vacancies are passivated[8–10]. For example, Teimouri et al.[10]

[1]Department of General Education (Physics and Mathematics), Faculty of Liberal Arts, Rajamangala University of Technology Rattanakosin, Wang Klai Kangwon Campus, Hua Hin , Prachuap Khiri Khan 77110, Thailand. [2]Department of Physics, Faculty of Science, Khon Kaen University, Khon Kaen 40002, Thailand. [3]Institute of Nanomaterials Research and Innovation for Energy (IN-RIE), Khon Kaen University, Khon Kaen 40002, Thailand. ✉email: ekaphan@kku.ac.th

synthesized Li-doped TiO_2 films that could show significantly improved conductivity with faster charge transfer in planar perovskite solar cells. Golvari et al.[11] prepared dye-sensitized solar cells on the mesoporous beads of Li-doped TiO_2 with 7.48% improvement of the device performance. The work of Lakra et al.[12] confirmed a good capacitive behavior of synthesized TiO_2 NPs and suggested the materials for SC electrodes application. Moreover, Wang et al.[13] suggested that the faradaic storage behavior of nanocrystalline anatase TiO_2 in aqueous electrolyte might be contributed to the conversion between Ti^{4+} and Ti^{3+} in the redox reaction. Meanwhile, the electrochemical properties of a symmetric hybrid SC with electrode of hydrothermally obtained SWCNTs/TiO_2 had been studied by Lal et al.[14], and the device delivered a high capacitance of 144 F g^{-1} with 20 Wh kg^{-1} of energy density and outstanding capacity retention of 95% after 50,000 cycles test. He et al.[15] fabricated a current collector of SC based on TiO_2 nanotube arrays (NTA) with a cathode of composite MnO_2/TiO_2 NTA, and attended a high capacitance of 1051 F cm^{-2}. Moreover, a value of 608.2 F cm^{-2} was accomplished in case of using Fe_2O_3 modified TiO_2 NTA as an anode, and the assembled asymmetric SC could retain about 91.7% capacitance after 5000 cycling tests. Another interesting material that had been considered as a promising applicant for efficient SCs electrode was heterostructure Co_3O_4/m-NTAs. In this study, Yu et al.[16] reported a maximum value of 662.7 F g^{-1} for specific capacitance with retain 86.0% of the value after 4000 cycles test at 10 A g^{-1}. Similarly, in the report of Li et al.[17], an assembled symmetric solid-state SC based on TiO_2-CNT electrodes could show a high value of 82.5 Wh kg^{-1} for energy density and 345.7 F g^{-1} at 1.0 A g^{-1} for specific capacitance. In addition, this TiO_2-CNT SC could demonstrate a good cycling stability of 93.3% for 10,000 cycling test, which might be due to the fast ion diffusion on surface of the anatase structure. Furthermore, Kumar et al.[18] found that a SC with carbon-supported TiO_2 electrode could exhibit a specific capacitance 277.72 F g^{-1} at 25 mV s^{-1} in 1 M Na_2SO_4 aqueous electrolyte. In addition, Elshahawy et al.[19] reported a value of 57.62 mF/cm for specific capacitance in 2 M KOH electrolyte of TiO_2 nanorod arrays based SCs, and could retain a capacity of 91% at the 10000th cycle of test. Ojha et al.[20] obtained the mesoporous Mn-doped TiO_2 by a simple sol–gel and a solvothermal method. According to this work, they suggested that the enhanced electrochemical properties could be mainly ascribed by many factors such as a larger surface area, a mesoporous structure and an appropriate concentration of Mn doping that could lead to the improved conductivity of a wide band gap TiO_2 NPs. Additionally, in the work of Hodaei et al.[21], nitrogen-doped TiO_2 NPs was obtained by a sol–gel process. The electrochemical study showed the enhanced capacitive performance, including a value of 311 F g^{-1} at 1 A g^{-1} for specific capacitance with remained 98.9% of the value after 4000 cycling tests. Regarding to the work of Hodaei et al.[21], the authors reported that a sol–gel method was an efficient process for preparing pure and metal-doped TiO_2 NPs to be applied for SCs electrode due to its unique chemical reaction that could yield high quality NPs. In addition, NPs of highly homogeneous size distribution with high surface area and very high purity (99.99%) could be obtained at a low temperature. Thus, a sol–gel synthesized metal-doped TiO_2 NPs is expected to play an important role for increasing electrical conductivity that can further improve the whole capacitive performance of supercapacitor[22,23].

Therefore, in this work, we focus on the electrochemical performance investigation of the as synthesized Li-doped anatase TiO_2 NPs ($Li_xTi_{1-x}O_2$ NPs, x = 0, 0.05, 0.10, 0.15 and 0.20) obtained by a sol–gel process. Interestingly, all $Li_xTi_{1-x}O_2$ NPs (x = 0.05–0.20) electrodes could demonstrate a pseudocapacitive behavior with a high specific capacitance and good cycling stability compared to undoped sample. To the best of our knowledge, it is the first time to fabricate SC with electrodes based on Li-doped TiO_2 NPs.

Experimental

Chemicals

Sigma Aldrich supplied titanium (IV) isopropoxide ($C_{12}H_{28}O_4Ti$, 99.95%), lithium hydroxide (LiOH, 99.50%), polyethylene glycol, ammonium hydroxide (NH_4OH, 99.50%), acetylene black (99.99%), polyvinylidene fluoride (PVDF) and ethanol (C_2H_5OH, 99%). Lithium sulfate (Li_2SO_4, 95%) is a product of Ajax Fine Chem Laboratory Chemicals. N-methyl-2-pyrrolidone (NMP, 99.5%) was obtained from RCI Labscan.

Synthesis of pure and Li-doped anatase TiO_2 NPs

In the process of synthesis pure anatase TiO_2 NPs, 5 ml polyethylene glycol was added to a well stirred deionized (DI) water:ethanol solution with 4:1 ratio by volume (40:10 ml). Then 10 ml of $C_{12}H_{28}O_4Ti$ was gradually dropped to this solution, while vigorously stirred at room temperature on a magnetic stirrer hot plate for further 20 min. Then, 2.5 wt.% aqueous ammonia (NH_4OH) was added dropwise to carefully controlled the pH at 7, and further stirring for 30 min. After that, increased the temperature of a solution to 60 °C and kept on stirring until a wet gel was formed, and allowed to dry at 75 °C. The final product was achieved by crushing the dried gel, ground to fine powder and pyrolized at 500 °C in a furnace for 2 h, using a heating rate of 2 °C/min. $Li_xTi_{1-x}O_2$ NPs (x = 0.05, 0.10, 0.15 and 0.20) was synthesized by a similar way, only that lithium hydroxide (LiOH) of 0.05, 0.10, 0.15 and 0.20 by wt % was added in the mixture solution before adding NH_4OH.

Electrodes fabrication for electrochemical properties study

The electrode slurries of $Li_xTi_{1-x}O_2$ NPs (x = 0, 0.05, 0.10, 0.15 and 0.20) were prepared by ball milling each product with PVDF and acetylene black at 80: 10: 10 wt% ratio in 500 µL NMP solvent at RT for 24 h. Each electrode was fabricated by dripping an active mass slurry of approximately 200 µL to coat on an area 1 cm^2 at one end of ultrasonically cleaned nickel foam sheet of size 1 × 2 cm^2, and dried for 2 h at 80 °C. After that, all electrodes were pressed at 1.5 tons for 1 min, and immersed in 0.5 M Li_2SO_4 aqueous electrolyte prior to electrochemical properties testing. The CV study was performed in an applied voltage of 0.0 to + 0.5 V at scan rate 10, 20, 30, 50, 100 and 200 mV s^{-1}. The GCD study was performed at applied current density 1.5, 2, 4, 6, 8, 10 and 15 A g^{-1}. The capacity retention was evaluated at the 2000th cycle of GCD test at 10 A g^{-1}. The GCD results were used for the calculation of specific capacitance (C_s) using Eq. (1)[24],

$$C_s = \frac{I\Delta t}{m\Delta V} \tag{1}$$

where I, Δt, m, and ΔV stand for the constant discharge current (A), discharge time (s), mass of active material in electrode (g) and potential window (V), respectively.

Additionally, the energy density (E_{sd}) and power density (P_{sd}) of electrodes were determined from the GCD results, using Eqs. (2) and (3)[24], respectively.

$$E_{sd} = \frac{C_s \times \Delta V^2}{7.2} \tag{2}$$

$$P_{sd} = \frac{E_{sd} \times 3600}{\Delta t} \tag{3}$$

Characterizations

X-ray source with CuKα (λ = 1.5406 Å) generated by X- ray diffractometer (Philips X'Pert) was used for crystal structure and phase identification of the products. Raman study using a laser of 532 nm excitation (DXR Smart, Thermo Scientific) was employed for TiO_2 phase verification. Moreover, in order to confirm the existence of various modes of vibration between Ti and O bonding in the TiO_2 crystalline structure, Fourier transform infrared spectroscopy (FTIR, Bruker, Senterra) was performed. The surface morphology inspection of products and particles size determination were accomplished by field emission scanning electron microscope (FE-SEM, FEI, Helios NanoLab G3 CX). In addition, the quantitative estimation for major elements in wt% of the products could be achieved using energy dispersive X-ray spectroscopy (EDS) with elemental mapping to display the distribution of elements. Furthermore, high magnified bright field images with selected area electron diffraction (SAED) patterns by transmission electron microscope (TEM, FEI, TECNAI G2 20) was performed for clearer observed products morphology and more accurate particles size determination, including phase and structure confirmation. An instrument of Autosorb1-Quantachrome was employed for the study of specific surface area and a type of pore distributed in samples through the Bruanauer Emmett-Teller (BET) and Barrett-Joyner-Halenda (BJH) techniques, respectively. Finally, an equipment of Wuhan Corrtest Instruments Corp Ltd. (Model CS350 Potentiostat/Galvanostat) was used for electrochemical properties studies of all $Li_xTi_{1-x}O_2$ NPs electrodes to obtain the CV, GCD and EIS results.

Results and discussion

The XRD patterns with Rietveld refinement fitting of $Li_xTi_{1-x}O_2$ NPs are displayed in Fig. 1a–e. In Fig. 1a–e, the most dominant XRD peaks at 25.26°, 36.92°, 47.96°, 53.92°, 55.01°, 62.83°, 70.24° and 75.04° correspond to the crystalline diffraction plane (101), (004), (200), (105), (211), (204), (116), and (215), respectively. The XRD results matched with the standard data of JCPDS: 21–1272 for the tetragonal anatase TiO_2 crystalline phase of space group: I41/amd[9,18,25]. However, in a sample of x = 0.15 and 0.20 (Fig. 1d, e), many peaks of monoclinic $Li_4Ti_5O_{12}$ phase with space group: C2/c observed at 17.32°, 30.95° and 44.49° correspond with the diffraction plane (111), (311) and (400), respectively, and matching to the standard data of JCPDS: 49-0207. The formation of $Li_4Ti_5O_{12}$ phase might be due to the direct interaction of excess Li with pure anatase crystalline TiO_2 phase during the growth process. It was suggested that this phase could provide a nonsymmetric stretching vibration of O–Ti–O that could result in reduced conductivity of the samples. Moreover, the cell parameter (a, b and c) with cell volume and various parameters (R_{wp}, R_p, R_{ex} and GOF, definition for these parameters was given elsewhere) were evaluated by Rietveld refinement method using a standard data of JCPDS: 21-1272 (tetragonal phase with space group: I41/amd) and JCPDS: 49-0207 (monoclinic phase with space group: C2/c), as displayed in Fig. 1a–e, and summarize of the results was listed in Table 1. As seen in Table 1 and the excellent fitting of the XRD patterns in Fig. 1a–e, it can be concluded that Li loading significantly affect the cell parameters of anatase TiO_2 phase. Obviously, the cell parameters and cell volume of samples decrease with increasing Li loading, leading to the deceased crystallite size of $Li_xTi_{1-x}O_2$ NPs. Generally, Ti^{4+} in a unit cell of TiO_2 crystal system is bonded to six equivalent O^{2-} atoms, leading to the formation of mixture distorted edge and corner-sharing TiO_6 octahedra. Furthermore, in a unit cell of $Li_4Ti_5O_{12}$ phase, a complicated structure is formed owing to the formation of LiO_4 tetrahedra by the bonding of Li^{1+} with four O^{2-} atoms at the cell corners that could be shared with others two equivalent LiO_6 octahedra and ten TiO_6 octahedra. Moreover, the percentage of anatase TiO_2 phase and $Li_4Ti_5O_{12}$ phase were determined in samples of x = 0.15 and 0.20, and found to be (95.12 and 4.88%) and (92.23 and 7.77%), respectively. Additionally, the X-ray line of the diffraction planes (101), (004), (200), (105), (211), (204), (116), and (215) were used for the evaluation of average crystallite sizes (D_{Sh}) of all samples, using the Scherrer's equation (4).

$$DSh = k\lambda/\beta \cos\theta, \tag{4}$$

In Eq. (4), the parameters θ, λ and β are defined for Bragg angle, wavelength of X-ray and full width at half maximum, respectively. k is the constant and was taken as 0.9. The evaluated D_{Sh} values are 19.61 ± 0.59, 19.21 ± 0.56, 18.31 ± 0.52, 18.23 ± 0.64 and 18.12 ± 0.76 nm for $Li_xTi_{1-x}O_2$ NPs of x = 0, 0.05 0.10, 0.15 and 0.20, respectively. All the D_{Sh} values were summarized in Table 1, and the plot of D_{Sh} versus Li concentration is illustrated in Fig. 1f. Obviously seen in Fig. 1f, D_{Sh} decreases with increasing Li concentration. The decreased D_{Sh} was suggested to originate from the replacement of a large ionic radius of Ti^{4+} (0.745 Å) and Ti^{3+} (0.670 Å) by a small ionic radius of Li^+ (0.60 Å) in the anatase TiO_2 crystal structure. By comparing the ionic radius of

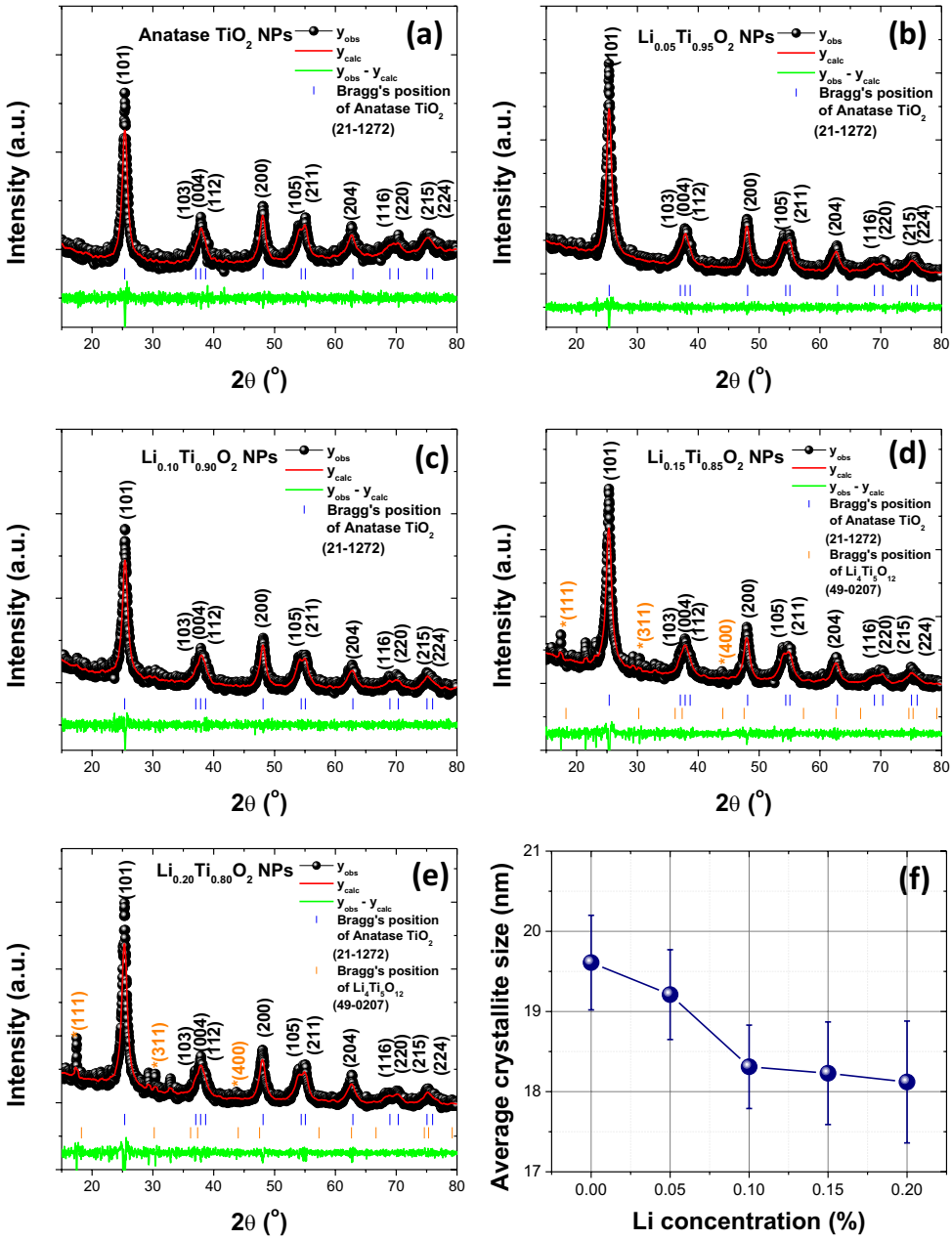

Figure 1. Rietveld refinement fitted XRD patterns of samples with different Li concentrations and plot of average crystallite size vs. Li concentration.

Li^+ (0.60 Å) and Ti^{4+} (0.745 Å), it is clear that a possible substitution of a small amount of Ti^{4+} by Li^+ would be accompanied by a weak lattice expansion, due to the relatively small difference between their respective ionic radius, so that the Li^+ ions can be dissolve into anatase TiO_2 phase and $Li_4Ti_5O_{12}$ phase[26]. However, the substitution might induce lattice expansion, resulting in a shift of the anatase peak to the lower angles. Although for the replacement of Ti^{4+} by L^{i+} ions, some Ti–O bonds are broken, which leads to the formation of oxygen vacancies, the contraction of lattice caused by oxygen deficiency is eliminated through lattice expansion induced by the presence of the slightly smaller lithium ions[11]. As a result, Li^+ ions appear to be an appropriate option for modifying the local crystal structure at Ti^{4+} sites in TiO_2, because they could operate as charge compensators and could additionally enhance capacitive properties due to the availability of more active sites[27].

FTIR spectra of samples are displayed in Fig. 2a–e. The broaden vibration peaks around 3250–3350 cm^{-1} are assigned for O–H stretching modes, relating to the stretching vibration of the hydroxyl (O–H) group due to the formation of H_2O molecules on surface[11]. Moreover, the appeared vibration peaks around 1640–1644 cm^{-1} are designated to the symmetric stretching of Ti–OH on surface[18]. Additionally, the observed peaks around 1110–1113 cm^{-1} and 600–625 cm^{-1} indicated the bonding of Ti–O in an anatase TiO_2 structure[11]. In the samples with x = 0.10, 0.15 and 0.20, the observed peaks in a range 790–900 cm^{-1} are attributed to the symmetric C–H

Parameter		Anatase TiO_2 NPs	$Li_xTi_{1-x}O_2$ NPs					
			x = 0.05,	x = 0.10,	x = 0.15		x = 0.20	
Space group		I41/amd	I41/amd	I41/amd	I41/amd	C2/c	I41/amd	C2/c
Crystal structure		Tetragonal	Tetragonal	Tetragonal	Tetragonal	Monoclinic	Tetragonal	Monoclinic
Crystalline parameter (Å)	*a*	3.78(3)	3.78 (3)	3.78(4)	3.77(4)	8.33(2)	3.77(2)	8.34(4)
	b	3.78 (2)	3.78 (2)	3.78 (4)	3.77(3)	8.33(2)	3.77(2)	8.34(4)
	c	9.51(3)	9.51(2)	9.50(4)	9.50(3)	13.14(4)	9.50(2)	13.17(1)
α = γ = β (°)		90	90	90	90	α = γ (90) β(108.1)	90	α = γ (90) β(107.9)
Cell volume (10^6 pm^3)		135.88	135.42	135.34	134.77	872.13	134.10	872.66
R_{ex} (%)		4.7331	5.3895	4.9934	5.2199		5.2424	
R_p (%)		4.5838	3.9797	4.0386	4.2830		4.6028	
R_{wp} (%)		6.0787	5.1291	5.2259	5.5440		6.0595	
GOF		6.0973	4.1996	3.1963	4.6255		4.1498	
D_{Sh} (nm)		19.61 ± 0.59	19.21 ± 0.56	18.31 ± 0.52	18.23 ± 0.64		18.12 ± 0.76	
% phase of TiO_2 and $Li_4Ti_5O_{12}$		100	100	100	95.12 4.88		92.23 7.77	
*D*ps (nm)		30.04 ± 4.92	27.97 ± 6.56	25.12 ± 2.64	25.03 ± 5.53		24.66 ± 6.13	
Specific surface area (m^2 g^{-1})		163.01	180.23	246.94	239.92		241.93	
Average pore-size (nm)		6.54 ± 0.93	6.31 ± 0.76	5.91 ± 0.66	5.71 ± 0.58		5.80 ± 0.61	
Pore volume (cm^3 g^{-1})		0.30	0.31	0.35	0.37		0.38	

Table 1. Cell parameters and phase analysis investigated by XRD and Rietveld refinement fitting with the results of surface and pore analysis of $Li_xTi_{1-x}O_2$ NPs.

and asymmetric CH_2 vibrations of an organic polyethylene glycol that could not be completely removed after calcination[11]. The strong vibration peaks in a range 410–625 cm^{-1} are associated with the vibration modes of O–Ti–O bonding in an anatase TiO_2 structure.

Further structural analysis of $Li_xTi_{1-x}O_2$ NPs (x = 0, 0.05, 0.10, 0.15 and 0.20) was performed by Raman technique, as shown in Fig. 3a–e. In these figures, the major sharp Raman shift observed at ~ 144 cm^{-1} corresponds to the $E_{g(1)}$ mode of anatase TiO_2[18,28]. The peak at 396 cm^{-1} corresponds to the $B_{1g(1)}$ mode, while another at 639 cm^{-1} corresponds to the $E_{g(2)}$ mode, arising from the symmetric stretching mode of O–Ti–O bonding in crystallite anatase TiO_2[28]. The other one observed at 515 cm^{-1} was assigned for $A_{1g} + B_{1g(2)}$ mode, corresponding to the antisymmetric bending vibration of O–Ti–O bonding in TiO_2 structure[18,28]. Therefore, Raman results confirmed the anatase phase of all samples.

Morphology and average particles size (*D*ps) of $Li_xTi_{1-x}O_2$ NPs are demonstrated by FE-SEM images with corresponding histograms in Fig. 4a–e. All images show the homogeneous distribution of agglomerated NPs with intercalated space between them, illustrating the micrographs of porous surface similar to spongy materials. However, a secondary monoclinic phase of $Li_4Ti_5O_{12}$ NPs that existed in the samples with x = 0.15 and 0.20 could not be observed or identified by SEM micrographs in Fig. d-1, d-2, e-1, e-2 was suggested to be owing to the small amount of them compared to a major TiO_2 phase, as estimated and listed in Table 1. The *D*ps values are 30.04 ± 4.92, 27.97 ± 6.56, 25.12 ± 2.64, 25.03 ± 5.53 and 24.66 ± 6.13 nm for samples of x = 0, 0.05 0.10, 0.15 and 0.20, respectively. The *D*ps values were listed in Table 1. As seen in Table 1, *D*ps decreases with increased Li loading. The uniform dispersion of agglomerated TiO_2 NPs in electrodes could lead to enhance the porosity and form the conducting networks for charge transfer, as suggested by Prashad et al.[20]. Moreover, the observed porous structure of Li-doped anatase TiO_2 NPs could increase the surface area of the electrode materials for the adsorption of electrolyte ions, resulting in more charges collection and could finally enhance the specific capacitance. Figure 5a–e display the EDS results and mapping of elements for $Li_xTi_{1-x}O_2$ NPs. The EDS results clearly show the uniform distribution of major elements Ti and O in the samples. However, Li element could not be detected due to its light-weight and a limitation of the instrument. The atomic percentages for Ti element were estimated to be about 55.0%, 53.7%, 52.9%, 50.9% and 50.5% for $Li_xTi_{1-x}O_2$ NPs with x = 0, 0.05 0.10, 0.15 and 0.20, respectively. The decreased amount of Ti was due to the Li replacement in anatase crystal structure of TiO_2.

In fact, more accurate particles size of $Li_xTi_{1-x}O_2$ NPs can be evaluated from TEM bright field images, including a better clear morphology of particles, as illustrated in Fig. 6a–e. As obviously seen, all images display NPs of very fine cuboidal shape with irregular size and agglomerated to form a spongy like-structure with roughly estimated individual particle size in an interval of 5–10 nm. Notably, the particle sizes estimated by TEM are smaller than those evaluated by SEM, which might be due to the dispersion of NPs during the sonication process of samples preparation prior to TEM performance. Moreover, the median size of NPs could be slightly reduced with the inclusion of Li^+ ions on the Ti^{4+} and Ti^{3+} sites in the anatase TiO_2 crystalline structure[18,20]. Furthermore, the unique morphology and homogenous size distribution in a narrow range of TiO_2 NPs was suggested to result in the increase of materials porosity and surface area. Additionally, the halo ring shape with arranged spots on the circumferences of SAED patterns in all samples indicate a polycrystalline nature of the materials[18]. Moreover, all SAED patterns had been indexed to be composed of different crystalline planes that correspond to those of anatase phase TiO_2, agreeing well with the XRD results shown in Fig. 1.

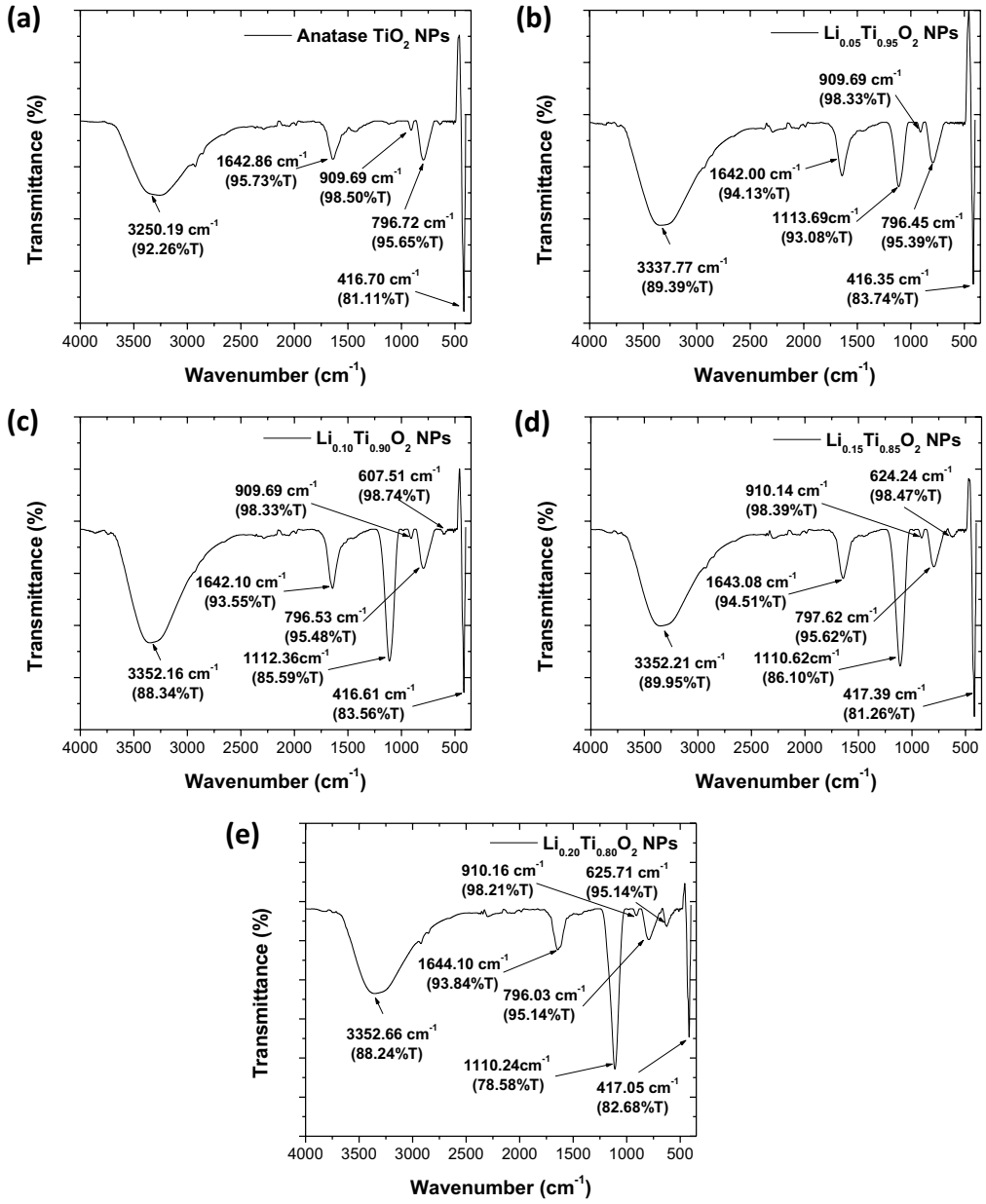

Figure 2. FTIR results of $Li_xTi_{1-x}O_2$ NPs with different Li concentrations.

Figure 7a–e display the N_2 adsorption/desorption isotherms results of $Li_xTi_{1-x}O_2$ NPs. Regarding to these results, the observed hysteresis loops of all samples exhibit the BET curve of type IV, corresponding to that of mesoporous materials[11,20]. The evaluated specific surface area of anatase TiO_2 NPs (x = 0) was 163.01 $m^2\ g^{-1}$, whereas those of $Li_xTi_{1-x}O_2$ NPs (x = 0.05, 0.10, 0.15 and 0.20) displayed the larger values of 180.23, 246.94, 239.92 and 241.93 $m^2\ g^{-1}$, respectively. Moreover, the average pore size and total specific pore volume of $Li_xTi_{1-x}O_2$ NPs (x = 0, 0.05, 0.10, 0.15 and 0.20) by the BJH technique were found to be 6.54 ± 0.93, 6.31 ± 0.76, 5.91 ± 0.66, 5.71 ± 0.58 and 5.80 ± 0.61 nm, and 0.30, 0.31, 0.35, 0.37 and 0.38 $cm^3\ g^{-1}$, respectively. All of these values were listed in Table 1, and their plots as a function of Li concentration are illustrated in Fig. 7f. It was suggested that the great increase of specific surface area with small pore size of Li-doped anatase TiO_2 NPs could create the appropriate pathways for ions to diffuse into the surface of electrodes, resulting in the increased charge collection and improvement of the capacitive performance[11,20]. The morphology and pore size of the produced compounds indicated nanoscale particles that could provide high electrolyte–electrode interfacial surface area, resulting in the comprehensive permeation of electrolyte and minimizing the path of transport to accelerate the fast transfer of Li^+ and e^- in Li-doped anatase TiO_2 NPs cathode[27]. Furthermore, the mesoporous nature of electrode could improve the access of electrolyte into the bulk of the materials, while also providing high power tapping densities and robust structural and electrical interconnectivity across the electrode[29].

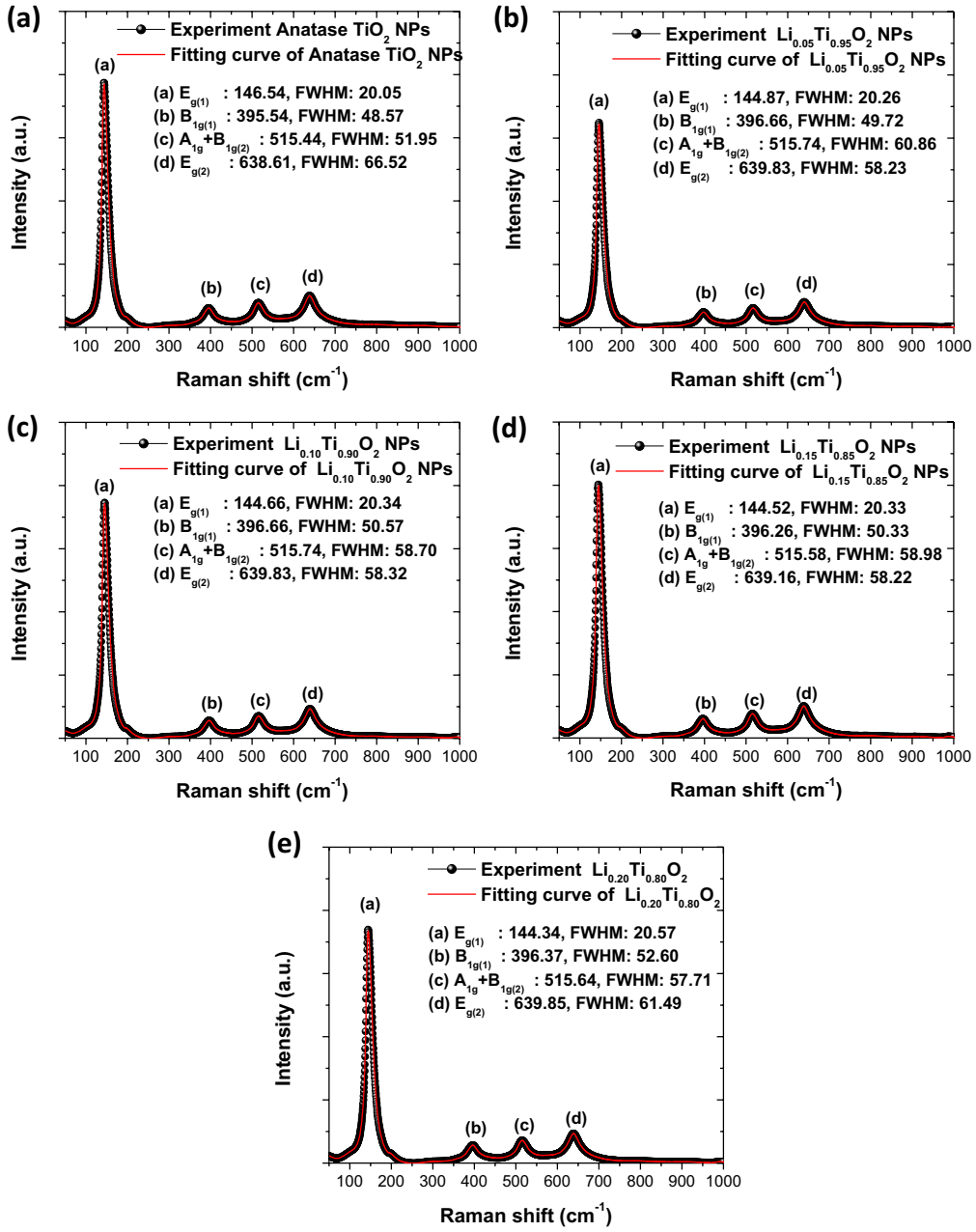

Figure 3. Raman results of $Li_xTi_{1-x}O_2$ NPs with different Li concentrations.

Cyclic voltammetry (CV) measurements of $Li_xTi_{1-x}O_2$ NPs (x = 0, 0.05, 0.10, 0.15 and 0.20) electrodes were performed at a scan rate 50 mV s^{-1} in 0.5 M Li_2SO_4 electrolyte within a potential window 0.0–0.5 V. The capacitive performance of each electrode is shown in Fig. 8a. The electrochemical performance of all electrodes performed at different scan rates are displayed in Fig. 8b–f. As seen in Fig. 8a, the CV curve of $Li_{0.10}Ti_{0.90}O_2$ NPs electrode reveals the largest size, indicating a superior electrochemical performance compared to other electrodes. According to Fig. 8a–f, the distorted rectangular shape with apparent redox peaks of CV curves are observed, suggesting a typical pseudocapacitive behavior of $Li_xTi_{1-x}O_2$ NPs electrodes[4,16,20]. Moreover, all curves exhibit the stability with increasing scan rate through the whole applied voltage range[4,18,20]. Additionally, it is obviously seen that with enhanced potential sweep rate from 10 to 200 mV s^{-1}, the anodic and cathodic peaks are shifted to the negative and positive values, respectively. In addition, the appeared anodic and cathodic peaks in a voltage range 0.18–0.35 V were due to the faradaic redox reaction of TiO_2 NPs. Generally, the appearance of redox peaks is correlated to the cation interaction on the TiO_2 surface, which can be expressed as[4,30]:

$$(TiO_2)surface + Li + + e- \leftrightarrow (TiO_2 - Li+)surface \quad (5)$$

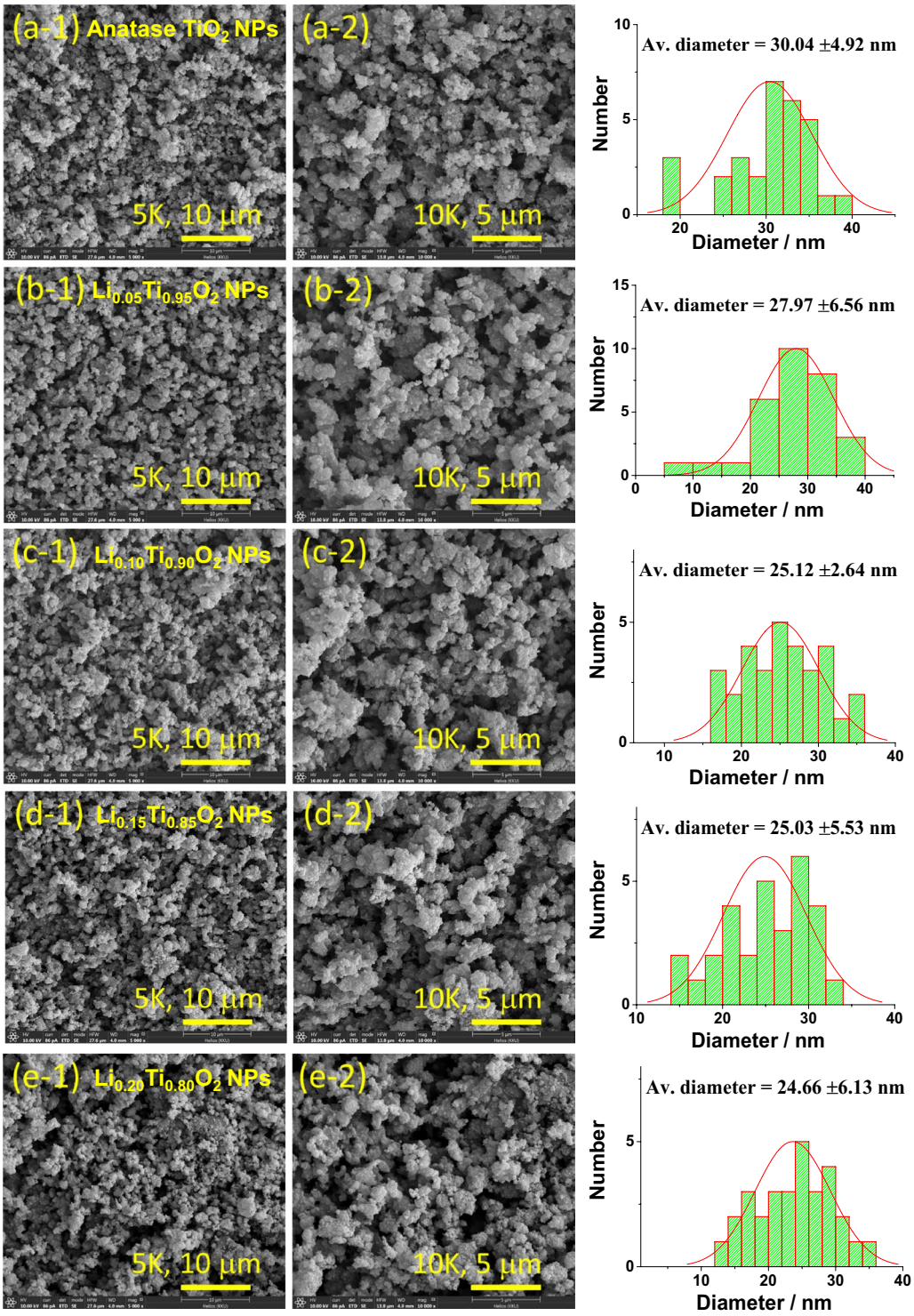

Figure 4. FE-SEM images (×5000 and ×10,000 magnification) and histograms for particles size distribution of $Li_xTi_{1-x}O_2$ NPs.

where Li^+ could be the Li_2SO_4 electrolyte. For CV curves of $Li_xTi_{1-x}O_2$ NPs electrodes displayed associated with Li^+ intercalation and de-intercalation into $Li_xTi_{1-x}O_2$ NPs electrodes. The overall cell reaction for the Li^+ insertion/extraction into $Li_xTi_{1-x}O_2$ NPs electrodes can be written as[4,30]:

$$(\mathrm{LixTi1-xO_2})surface + \mathrm{Li++e-} \leftrightarrow (\mathrm{Lix(Ti4+/Ti3+)1-xO_2-Li+})surface \quad (6)$$

Owing to the excellent ability of alteration between different oxidation states of Ti ions during the redox reaction, TiO_2 was suggested to be a potential material for SCs electrode. Regarding to the redox reaction,

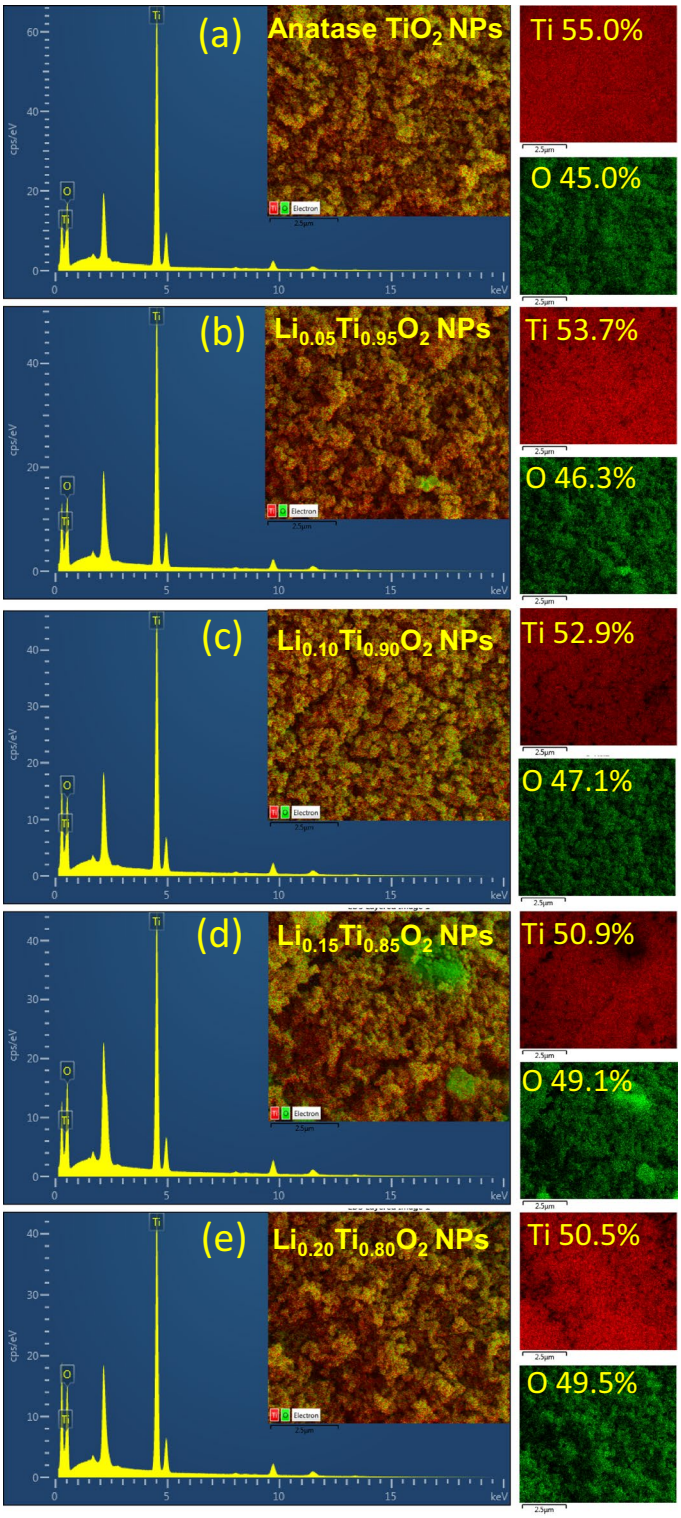

Figure 5. EDS results and mapping images of $Li_xTi_{1-x}O_2$ NPs.

Ti^{4+} was transferred to Ti^{3+} while charging, and converted to the initial state during discharging[18,19], showing a pseudocapacitive behavior of n-type semiconductor for all $Li_xTi_{1-x}O_2$ NPs electrodes. In addition, it was reported that during discharge, a number of Li^+ ions was inserted into the interstitial sites of the Li-doped TiO_2 NPs framework, which implied a partial reduction of Ti^{4+} to Ti^{3+} state[29,31–34]. Moreover, it was also suggested that the redox reaction could be possibly affected by the thickness variation of diffusion layers in electrodes due to using different scan rates in the measurements. The obviously enhanced current with scan rates indicates a good rate capability of $Li_{0.10}Ti_{0.90}O_2$ NPs electrode. While the conductivity of electrodes with higher Li concentration

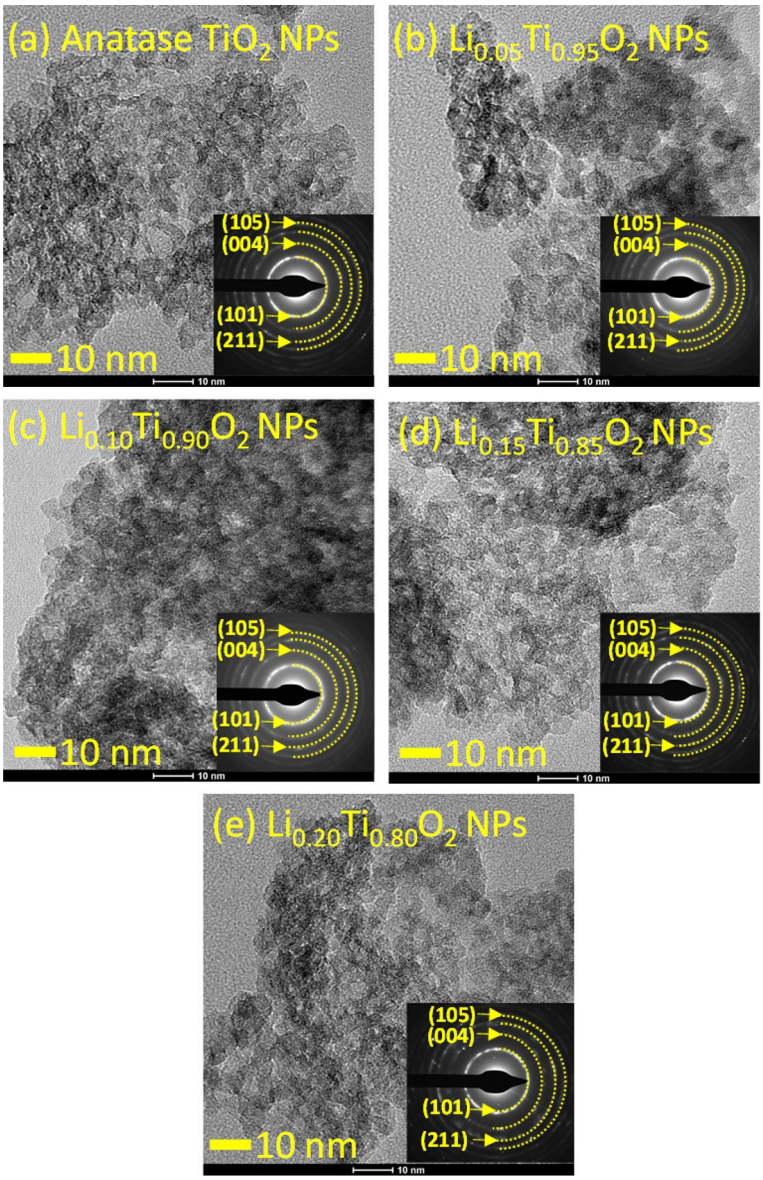

Figure 6. TEM bright field images with insets showing indexed SAED patterns of $Li_xTi_{1-x}O_2$ NPs.

(x = 0.15 and 0.20) was observed to decrease, suggesting to be affected by the defect sites generated by the presence of $Li_4Ti_5O_{12}$ phase in the materials.

For further investigation of electrochemical properties of $Li_xTi_{1-x}O_2$ NPs electrodes, the galvanostatic charge discharge (GCD) measurements were performed at 1.5 A g^{-1}, and the results are displayed in Fig. 9a. In addition, more GCD results performed with variation of current density from 1.5 to 15 A g^{-1} for each electrode are displayed in Fig. 9b–f. In these figures, GCD curves of all electrodes illustrate a non-symmetrical voltage–time profile at each constant current density, indicating a pseudocapacitive behavior with superior electrochemical reversibility through the whole charge/discharge process[4,18,20]. The maximum specific capacitance (C_s) at 1.5 A g^{-1} of 822 F g^{-1} was achieved in $Li_xTi_{1-x}O_2$ NPs electrode with x = 0.10, while the C_s values of others electrode with x = 0, 0.05, 0.15 and 0.20 were evaluated to be 513, 666, 747 and 579 F g^{-1}, respectively, as displayed in Fig. 10a, and summarized in Table 2. The longer discharge time than other electrodes at 1.5 A g^{-1} (see Fig. 9b–f) suggests a good electrochemical performance of Li-doped TiO_2 Nps electrode with 0.10% Li loading. The GCD profile of $Li_{0.10}Ti_{0.90}O_2$ NPs electrode, displaying a good performance with the highest C_s value, is in good agreement with its CV results shown in Fig. 8a, d. Generally, P_{sd} and E_{sd} obtained by the Ragone plot are two other important parameters used for evaluating the supercapacitor performance. Accordingly, Fig. 10b displays the Ragone plots of all $Li_xTi_{1-x}O_2$ NPs electrodes, illustrating the decreased P_{sd} and E_{sd} values with increasing current density, which might be correlated to the limit of ions diffusion in electrodes and electrolyte[21]. The energy density (E_{sd}) and power density (P_{sd}) at 1.5 A g^{-1} of $Li_xTi_{1-x}O_2$ NPs electrodes (x = 0, 0.05, 0.10, 0.15 and 0.20) are (64.12, 83.25, 102.75, 93.38 and 72.37 W h kg^{-1}), and (51.04, 66.67, 176.04, 104.16 and 51.04 W kg^{-1}), respectively. As seen, all Li-doped anatase TiO_2 NPs electrodes revealed the improved P_{sd} and E_{sd} as compared to that of undoped anatase

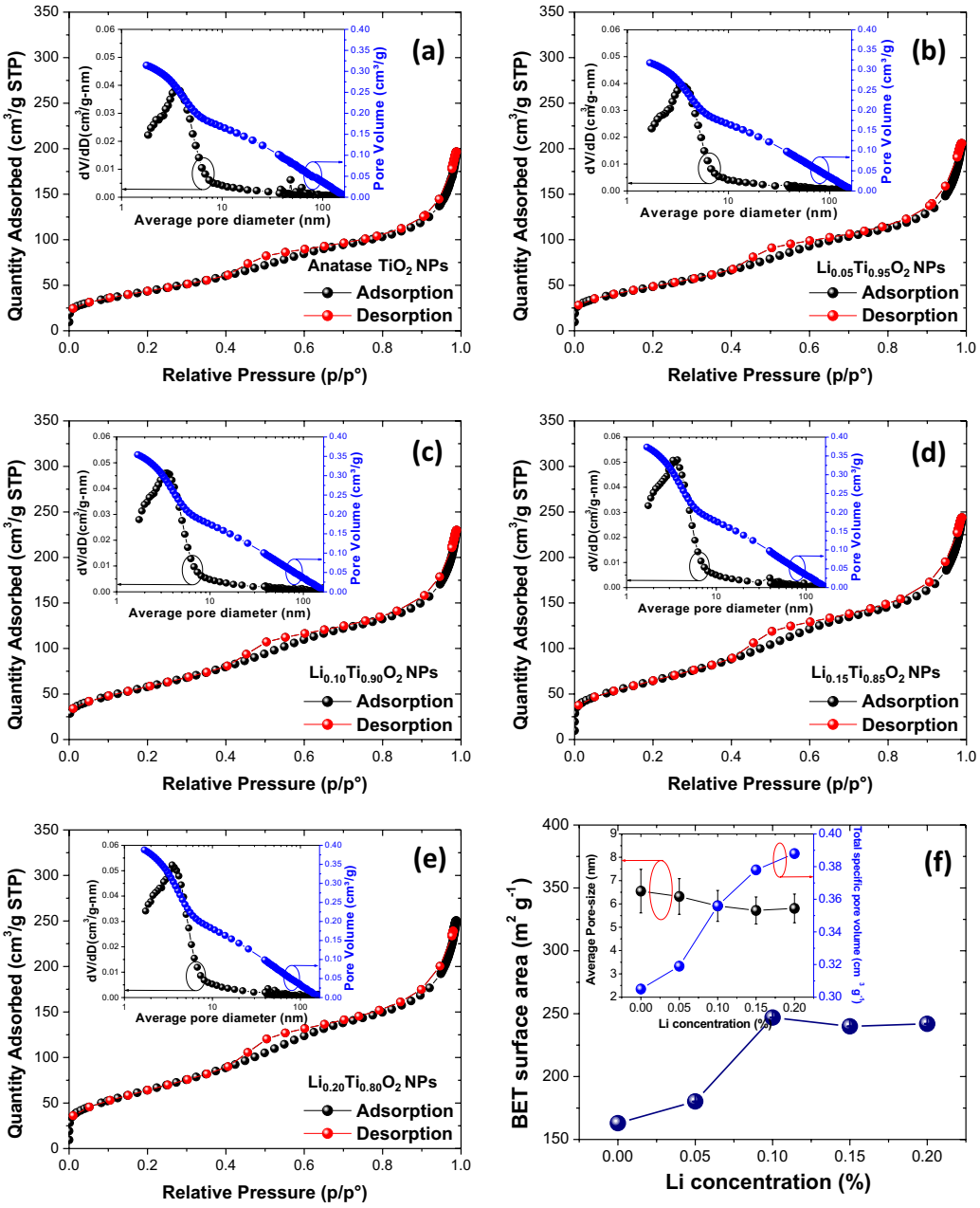

Figure 7. (**a–e**) Nitrogen sorption isotherms results with inset showing average pore diameter of $Li_xTi_{1-x}O_2$ NPs. (**f**) Plots of BET surface area, average pore size and total specific pore volume (inset) as a function of Li concentration.

TiO_2 NPs electrode. The increased electrical conductivity and surface area of Li-doped anatase TiO_2 NPs with increasing Li content were suggested for the improved performance. Furthermore, the GCD results for electrochemical stability study at 10 A g^{-1} with 5000 cycles test are illustrated in Fig. 10c. According to these results, a high capacitance retention of 87.1%, 89.0%, 92.6%, 91.7% and 90.4% at the 5000th cycles were attained for $Li_xTi_{1-x}O_2$ NPs electrodes with x = 0, 0.05, 0.10, 0.15 and 0.20, respectively, and the values were listed in Table 2. Obviously, all electrodes of Li-doped anatase TiO_2 NPs illustrated a superior capacitance retention as compared to undoped anatase TiO_2 NPs[18]. Actually, it has been observed that good stability after testing for 5000th cycles of all $Li_xTi_{1-x}O_2$ NPs electrodes in aqueous electrolyte of 0.5 M Li_2SO_4 is the most interesting one, since three main effects are evident; (i) decrease in the aggregation and overlapping of $Li_xTi_{1-x}O_2$ NPs during a long time required by the charge–discharge process, (ii) the fast Li^+ ions diffusion and increased electronic conductivity on surface of $Li_xTi_{1-x}O_2$ NPs, and (iii) a slight shift of the CV and GCD curves is a very promising strategy to produce an environment friendly supercapacitor, which is able to reach in the future for the targeted energy and power density of organic electrolyte-based systems with acceptable good electrochemical performance[35–38]. Additionally, the EIS results of all $Li_xTi_{1-x}O_2$ NPs electrodes obtained in a range 0.01–100 kHz frequency at

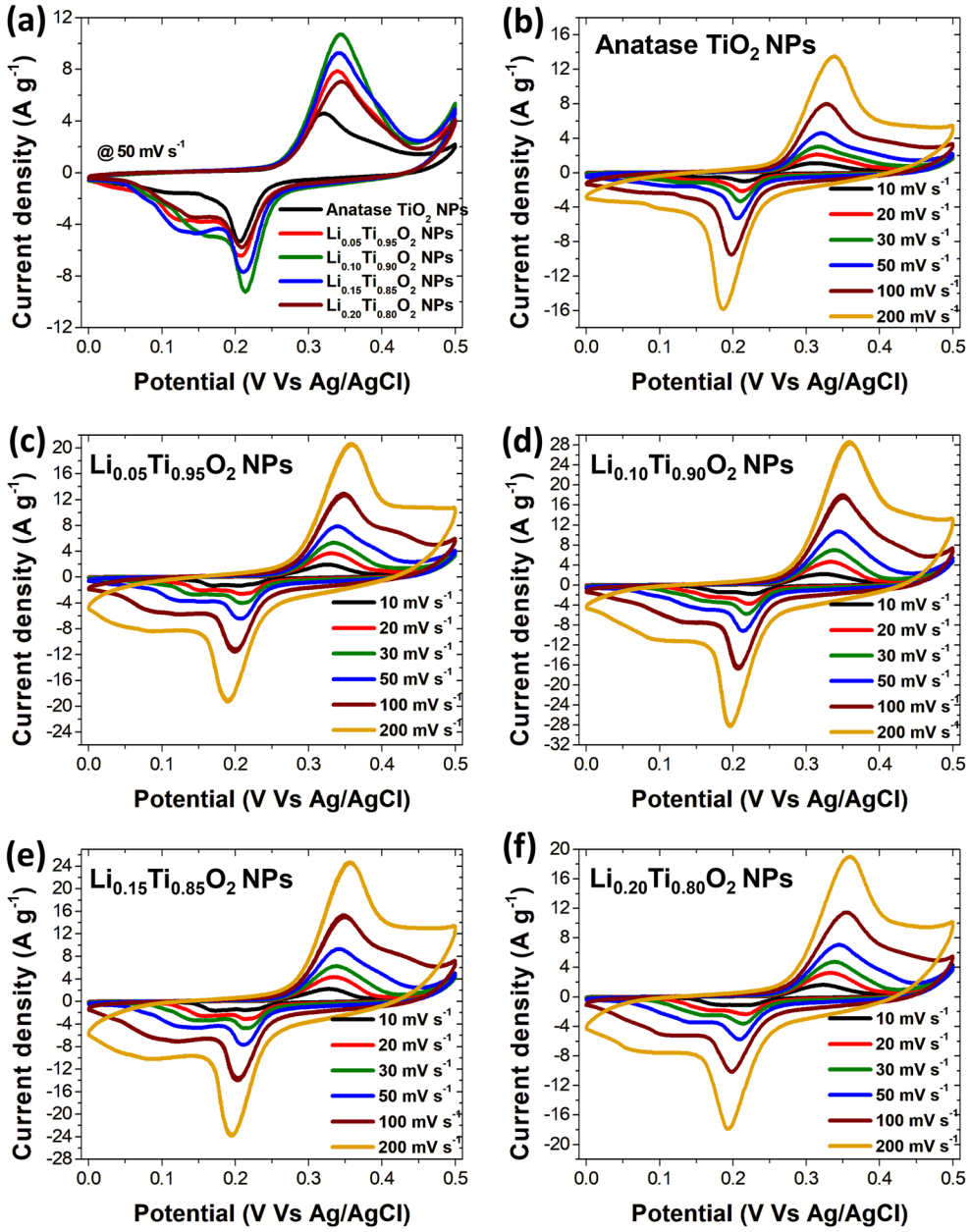

Figure 8. CV curves of $Li_xTi_{1-x}O_2$ NPs electrodes.

5 mV are shown in Fig. 10d, and all the obtained data were provided in Table 2. Next, the series resistance (R_s) of $Li_xTi_{1-x}O_2$, NPs electrodes with x = 0, 0.05, 0.10, 0.15 and 0.20 were determined to be 4.05, 4.03, 4.11, 4.10 and 4.03 Ω, respectively. Moreover, Li-doped anatase TiO_2 NPs electrodes showed the low Rct value evaluated from a semicircle part in a high frequency region near the origin of the plots, meanwhile the plots connected to a low frequency region show almost the incline straight lines parallel to Z" (Ω)[4,18,20,21]. As results, this might cause the formation of more vacancy sites in TiO_2 lattice as well as the faster charge transferability in the Li-doped anatase TiO_2 NPs electrodes, ascribed primarily due to the change of the intrinsic conductive properties of TiO_2 NPs due to Li doping[18,20]. For Warburg resistance (W_R), which describes the ion diffusion process of redox materials, the W_R values for all electrodes in a low frequency range were generally evaluated from the slopes of Z" plots that abruptly increase in a straight line next to a high frequency region. As seen in Table 2, the W_R value of $Li_xTi_{1-x}O_2$ NPs electrode with x = 0.10 is lower than those of other electrodes. The lower value of W_R implies the faster ion transferability from electrolyte to electrode, resulting in a greater C_s value[18,20]. The EIS results clearly indicate the decreased series resistance of Li-doped anatase TiO_2 NPs electrodes as compared with the bare anatase TiO_2 NPs electrode. Regarding to the ascribed results, it was suggested that $Li_xTi_{1-x}O_2$ NPs with x = 0.10 was an appropriate material to be applied for electrode of high-performance supercapacitors. To express the excellent and attractive capacitive value of $Li_{0.10}Ti_{0.90}O_2$ NPs electrode, the comparison of its electrochemical performance with others TiO_2-based electrode was illustrated in Table 3. Therefore, in this study, we thoroughly explored the influence of

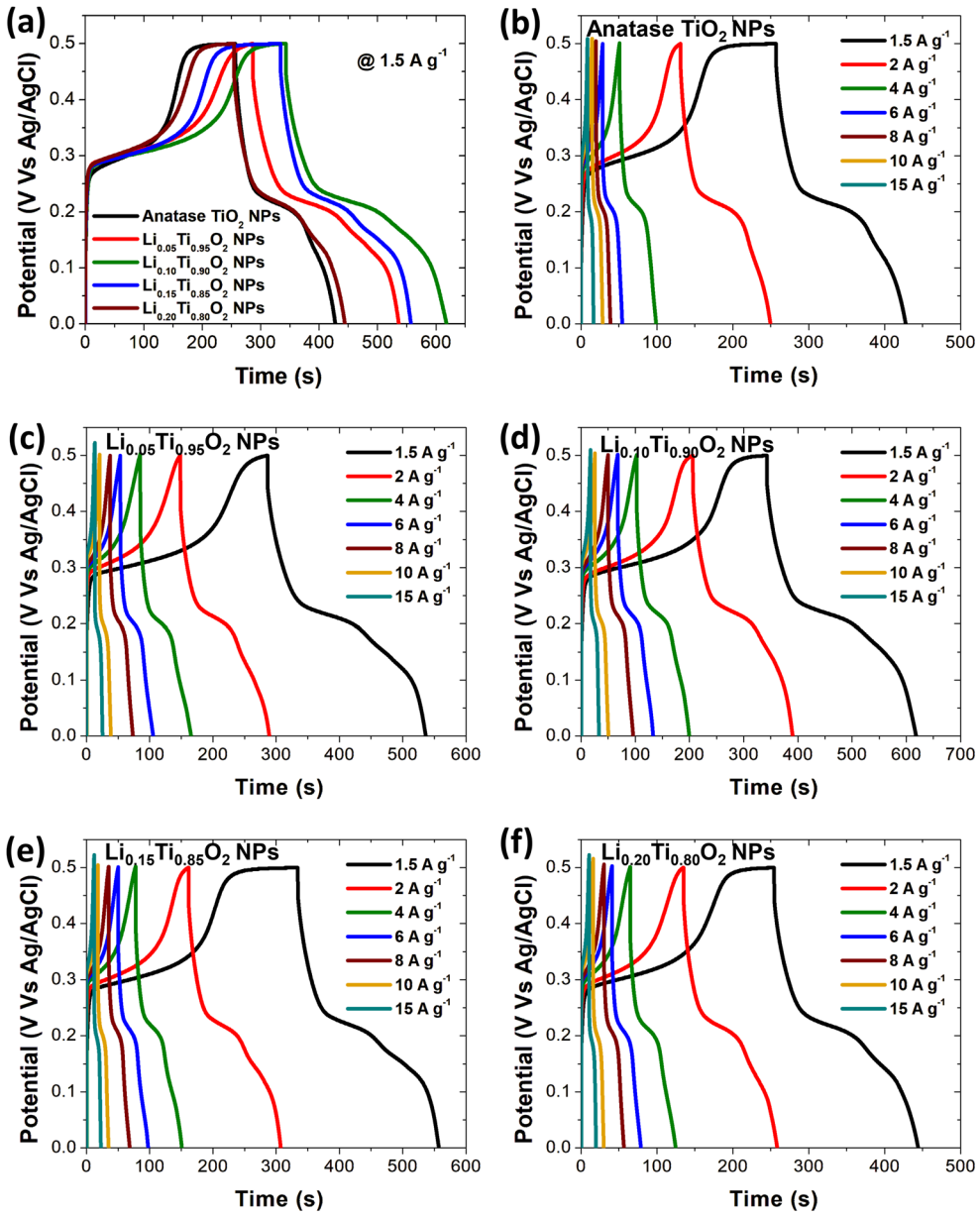

Figure 9. (**a**) GCD results of all $Li_xTi_{1-x}O_2$ NPs electrodes at 1.5 A g^{-1}. (**b–f**) GCD results of all $Li_xTi_{1-x}O_2$ NPs (x = 0.0–0.20) electrodes performed at different current densities.

Li-doped anatase-TiO_2 NPs on high-performance supercapacitors. Generally, pentavalent donor-type doping is required to increase the material's electrical conductivity, and Li^+ ions can easily substitute Ti^{4+} and Ti^{3+} ions in the anatase-TiO_2 lattice at a wide range of concentrations. According to the experimental results, adding a modest amount of Li to the material could potentially affect many factors such as crystal size, phase purity, morphology, surface area, and pore size distribution. Consequently,$Li_xTi_{1-x}O_2$ NPs electrode with x = 0.10 exhibited superior ion diffusivity, high conductivity, and small particle size compared to the other samples. As a result, $Li_{0.10}Ti_{0.90}O_2$ NPs electrode exhibited a higher electrochemical activity compared to the others electrode. The increased lattice parameters could improve its overall performance by enhancing its metallic-like character, while having minor effects on its electrochemical properties. The CV and GCD tests showed that the $Li_{0.10}Ti_{0.90}O_2$ NPs electrode exhibited a pseudocapacitive storing mechanism, which occurred on the electrode surfaces at Li-doped Ti sites. As a result, Li^+ ions played an important role in the improvement of electrical conductivity, charge storage capacity and stability with capacitance retention reaching as high as 92.6% after 5,000 cycles GCD test.

Conclusions

In summary, anatase $Li_xTi_{1-x}O_2$ NPs (x = 0, 0.05 0.10, 0.15 and 0.20) could be synthesized by the sol–gel process. The anatase phase with space group I41/amd of tetragonal $Li_xTi_{1-x}O_2$ NPs was confirmed by XRD results. Additionally, the monoclinic phase of $Li_4Ti_5O_{12}$ was detected in samples with x higher than 0.10, suggesting for the

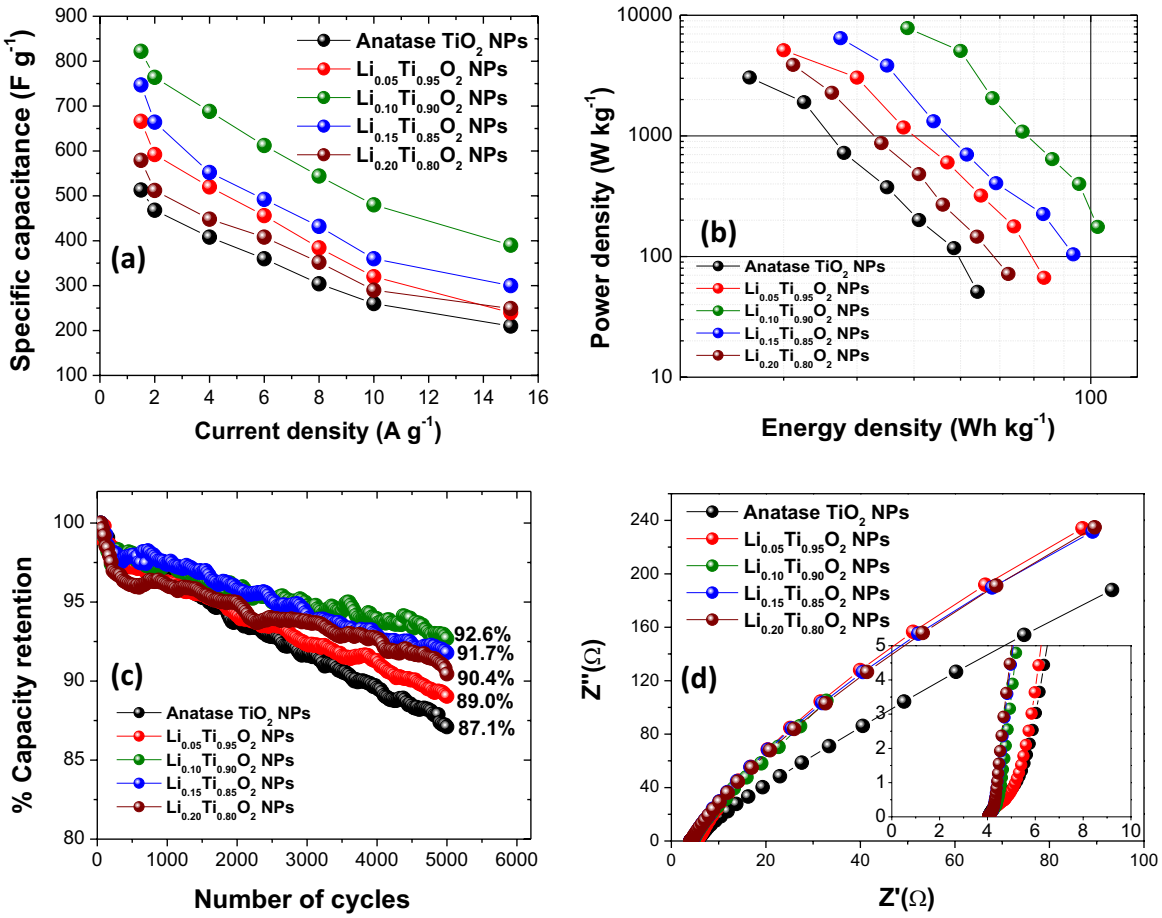

Figure 10. Electrochemical performance of all electrodes, (**a**) specific capacitance vs. current density, (**b**) Ragone plots, (**c**) cycling stability at 10 A g^{-1} and (**d**) Nyquist plots of all electrodes in aqueous electrolyte of 0.5 M Li_2SO_4.

Parameter		Anatase TiO_2 NPs (x = 0.0)	$Li_xTi_{1-x}O_2$ NPs			
			x = 0.05,	x = 0.10	x = 0.15	x = 0.20
C_s (F g^{-1})	1.5 A g^{-1}	513	666	822	747	579
	2 A g^{-1}	468	592	764	664	512
	4 A g^{-1}	408	520	688	552	448
	6 A g^{-1}	360	456	612	492	408
	8 A g^{-1}	304	384	544	432	352
	10 A g^{-1}	260	320	480	360	290
	15 A g^{-1}	210	240	390	300	249
(%) Capacity retention at 10 A g^{-1} after 5000 cycles		87.1	89.0	92.6	91.7	90.4
Energy density (W h kg^{-1}) at 1.5 A g^{-1}		64.12	83.25	102.75	93.38	72.37
Power density (W kg^{-1}) at 1.5 A g^{-1}		51.04	66.67	176.04	104.16	51.04
EIS analysis	R_s (Ω)	4.05	4.03	4.11	4.10	4.03
	R_{ct} (Ω)	0.86	0.80	0.56	0.43	0.31
	W_R	2.95	2.86	2.34	2.72	2.74

Table 2. C_s values and capacity retention with energy density, power density and EIS analysis of all $Li_xTi_{1-x}O_2$ NPs (x = 0.0–0.20) electrodes.

reduced conductivity and electrochemical performance of samples. Raman spectra demonstrated characteristic peaks that represented the anatase phase of TiO_2 in all samples. Moreover, FT-IR spectra also confirmed the existence of different modes of vibration between Ti and O atoms in the TiO_2 structure. TEM and FE-SEM images revealed the homogeneously dispersed Li-doped TiO_2 NPs in a spongy like morphology with estimated particles size in a range 5–10 nm by TEM. Such a morphology was suggested to enhance the porosity, and to form an excellent conducting

Electrode	Synthesis method	Electrolyte	C_s	Current density or scan rate	Capacity retention (number of cycle test)
AC/TiO_2 electrode[7]	Hydrothermal method	0.5 M NaCl	515 mF/cm^2	5 mV s^{-1}	–
Homogeneous Co_3O_4/TiO_2 nanotube electrode[16]	Chemical bath deposition (CBD)	2 M KOH	662 F g^{-1}	1 A g^{-1}	86% (4000)
TiO_2 with Kapton tape, annealed under air[19]	Hydrothermal method	2 M KOH	57.62 F/cm^2	10 mV s^{-1}	90% (10,000)
Mn-TiO_2 electrode[20]	Hydrothermal method	1 M Na_2SO_4	328 F g^{-1}	5 A g^{-1}	84% (2000)
N-doped TiO_2 electrode[21]	Sol–gel method	3.0 M KCl	311 F g^{-1}	1 A g^{-1}	98.9% (4000)
Black TiO_2 electrode[39]	Electrochemical self-doping	1 M Na_2SO_4	15.6 mF/cm^2	100 mV s^{-1}	96% (5000)
TiO_2@C NRAs electrode[40]	Anodization process	0.5 M Na_2SO_4	23.6 mF/cm^2	5 mV s^{-1}	91% (1000)
The hollow N-TiO_2 shells electrode[41]	Sol–gel method	1 M Na_2SO_4	2.48 mF/cm^2	10 mV s^{-1}	88.7% (1000)
$Li_{0.10}Ti_{0.90}O_2$ NPs electrode This work	Sol–gel method	0.5 M Li_2SO_4	822 F g^{-1}	1.5 A g^{-1}	92.6% (5000)

Table 3. Electrochemical performance comparison of TiO_2-based electrodes synthesized by different methods, performed in different electrolytes and current densities or scan rates.

network of NPs for charges transfer. The BET results illustrated the increased surface area of $Li_xTi_{1-x}O_2$ NPs with increasing Li loading. Electrochemical studies showed the pseudocapacitive behavior of all samples with high-quality performance achieved in a sample of x = 0.10 that revealed the highest value of 822 F g^{-1} for specific capacitance at 1.5 A g^{-1}, and could retain 92.6% of its original value after 5000 cycles test. Therefore, $Li_{0.10}Ti_{0.90}O_2$ NPs with excellent performance in terms of high capacitance, high power density (176.04 W kg^{-1}) and high energy density (102.75 W h kg^{-1}) was suggested to be an appropriate material for supercapacitors electrodes application.

Received: 17 February 2024; Accepted: 13 May 2024
Published online: 16 May 2024

References

1. Xie, K. *et al.* Carbon nanocages as supercapacitor electrode materials. *Adv. Mater.* **24**, 347–352. https://doi.org/10.1002/adma.201103872 (2012).
2. Augustyn, V., Simon, P. & Dunn, B. Pseudocapacitive oxide materials for high-rate electrochemical energy storage. *Energy Environ. Sci.* **7**, 1597–1614. https://doi.org/10.1039/C3EE44164D (2014).
3. Zhang, S. & Pan, N. Supercapacitors performance evaluation. *Adv. Energy Mater.* **5**, 1401401. https://doi.org/10.1002/aenm.201401401 (2015).
4. Naeem, F. *et al.* TiO_2 nanomembranes fabricated by atomic layer deposition for supercapacitor electrode with enhanced capacitance. *Nanoscale Res. Lett.* **14**, 92. https://doi.org/10.1186/s11671-019-2912-3 (2019).
5. Ullattil, S. G., Narendranath, S. B., Pillai, S. C. & Periyat, P. Black TiO_2 nanomaterials: A review of recent advances. *Chem. Eng. J.* **343**, 708–736. https://doi.org/10.1016/j.cej.2018.01.069 (2018).
6. Selvakumar, M. & Bhat, D. K. Microwave synthesized nanostructured TiO_2-activated carbon composite electrodes for supercapacitor. *Appl. Surf. Sci.* **263**, 236–241. https://doi.org/10.1016/j.apsusc.2012.09.036 (2012).
7. Barakat, N. A. M., Sayed, Y. T., Irfan, O. M. & Abdelaty, M. M. Synthesis of TiO_2-incorporated activated carbon as an effective Ion electrosorption material. *PLOS ONE* **18**, e0282869. https://doi.org/10.1371/journal.pone.0282869 (2023).
8. Roose, B., Pathak, S. & Steiner, U. Doping of TiO_2 for sensitized solar cells. *Chem. Soc. Rev.* **44**, 8326–8349. https://doi.org/10.1039/C5CS00352K (2015).
9. Panday, M., Upadhyay, G. K. & Purohit, L. P. Effect of Li doping on passivation of trap states and improvement in charge transport in TiO_2 thin films. *Pramana* **95**, 132. https://doi.org/10.1007/s12043-021-02167-0 (2021).
10. Teimouri, R. *et al.* Synthesizing Li doped TiO_2 electron transport layers for highly efficient planar perovskite solar cell. *Superlattices Microstruct.* **145**, 106627. https://doi.org/10.1016/j.spmi.2020.106627 (2020).
11. Golvari, P., Nouri, E., Mohsenzadegan, N., Mohammadi, M. R. & Martinez-Chapa, S. O. A single layer deposition of Li-doped mesoporous TiO_2 beads for low-cost and efficient dye-sensitized solar cells. *New J. Chem.* **45**, 2470–2477. https://doi.org/10.1039/D0NJ04051G (2021).
12. Lakra, R., Kumar, R., Kumar, S., Thatoi, D. & Soam, A. Synthesis of TiO_2 nanoparticles as electrodes for supercapacitor. *Mater. Today Proc.* **74**, 863–866. https://doi.org/10.1016/j.matpr.2022.11.271 (2023).
13. Wang, J., Polleux, J., Lim, J. & Dunn, B. Pseudocapacitive contributions to electrochemical energy storage in TiO_2 (anatase) nanoparticles. *J. Phys. Chem. C* **111**, 14925–14931. https://doi.org/10.1021/jp074464w (2007).
14. Lal, M. S., Badam, R., Matsumi, N. & Ramaprabhu, S. Hydrothermal synthesis of single-walled carbon nanotubes/TiO_2 for quasi-solid-state composite-type symmetric hybrid supercapacitors. *J. Energy Storage* **40**, 102794. https://doi.org/10.1016/j.est.2021.102794 (2021).
15. He, Z.-K. *et al.* Surface-charge regulated TiO_2 nanotube arrays as scaffold for constructing binder-free high-performance supercapacitor. *Appl. Surf. Sci.* **567**, 150832. https://doi.org/10.1016/j.apsusc.2021.150832 (2021).
16. Yu, C. *et al.* Supercapacitive performance of homogeneous Co_3O_4/TiO_2 nanotube arrays enhanced by carbon layer and oxygen vacancies. *J. Solid State Electrochem.* **21**, 1069–1078. https://doi.org/10.1007/s10008-016-3441-y (2017).
17. Li, J., Ao, J., Zhong, C. & Yin, T. Three-dimensional nanobranched TiO_2-carbon nanotube for high performance supercapacitors. *Appl. Surf. Sci.* **563**, 150301. https://doi.org/10.1016/j.apsusc.2021.150301 (2021).
18. Kumar, R. *et al.* In situ carbon-supported titanium dioxide (ICS-TiO_2) as an electrode material for high performance supercapacitors. *Nanoscale Adv.* **2**, 2376–2386. https://doi.org/10.1039/D0NA00014K (2020).
19. Elshahawy, A. M., Elkatlawy, S. M., Shalaby, M. S., Guan, C. & Wang, J. Surface-engineered TiO_2 for high-performance flexible supercapacitor applications. *J. Electron. Mater.* **52**, 1347–1356. https://doi.org/10.1007/s11664-022-10084-0 (2023).
20. Prashad Ojha, D., Babu Poudel, M. & Joo Kim, H. Investigation of electrochemical performance of a high surface area mesoporous Mn doped TiO_2 nanoparticle for a supercapacitor. *Mater. Lett.* **264**, 127363. https://doi.org/10.1016/j.matlet.2020.127363 (2020).
21. Hodaei, A., Dezfuli, A. S. & Naderi, H. R. A high-performance supercapacitor based on N-doped TiO_2 nanoparticles. *J. Mater. Sci. Mater. Electron.* **29**, 14596–14604. https://doi.org/10.1007/s10854-018-9595-x (2018).

22. Hejazi, S., Pour-Ali, S., Killian, M. S. & Mohajernia, S. One-dimensional suboxide TiO_2 nanotubes for electrodics applications. *Electrochem. Commun.* **136**, 107246. https://doi.org/10.1016/j.elecom.2022.107246 (2022).
23. Zhang, L. *et al.* The electrode materials of supercapacitor based on TiO_2 nanorod/MnO_2 ultrathin nanosheet core/shell arrays. *J. Nanomater.* **2020**, 6642236. https://doi.org/10.1155/2020/6642236 (2020).
24. Zou, K. *et al.* Insights into enhanced capacitive behavior of carbon cathode for lithium ion capacitors: The coupling of pore size and graphitization engineering. *Nano-Micro Lett.* **12**, 121. https://doi.org/10.1007/s40820-020-00458-6 (2020).
25. Slimani, Y. *et al.* Synthesis of Ce and Sm co-doped TiO_2 nanoparticles with enhanced photocatalytic activity for rhodamine B dye degradation. *Catalysts* **13**, 668 (2023).
26. Tamarani, A., Zainul, R. & Dewata, I. Preparation and characterization of XRD nano Cu-TiO_2 using sol-gel method. *J. Phys. Conf. Ser.* **1185**, 012020. https://doi.org/10.1088/1742-6596/1185/1/012020 (2019).
27. Liao, J.-Y. *et al.* Hierarchical $Li_4Ti_5O_{12}$-TiO_2 composite microsphere consisting of nanocrystals for high power Li-ion batteries. *Electrochim. Acta* **108**, 104–111. https://doi.org/10.1016/j.electacta.2013.06.073 (2013).
28. Scepanovic, M. *et al.* Characterization of La-doped TiO_2 nanopowders by Raman spectroscopy. *Acta Phys. Polon. Ser. A* **115**, 771–774. https://doi.org/10.12693/APhysPolA.115.771 (2009).
29. Lakshmi-Narayana, A. *et al.* Electrochemical performance of Li_2TiO_3//$LiCoO_2$ li-ion aqueous cell with nanocrystalline electrodes. *Batteries* **8**, 149 (2022).
30. Yang, S., Lin, Y., Song, X., Zhang, P. & Gao, L. Covalently coupled ultrafine H-TiO_2 nanocrystals/nitrogen-doped graphene hybrid materials for high-performance supercapacitor. *ACS Appl. Mater. Interfaces* **7**, 17884–17892. https://doi.org/10.1021/acsami.5b04368 (2015).
31. Kuang, Y. *et al.* Fabrication and electrochemical investigation of $Li_{0.5}TiO_2$ as anode materials for lithium ion batteries. *Ionics* **23**, 3265–3271. https://doi.org/10.1007/s11581-017-2148-0 (2017).
32. Shenouda, A. Y. & Murali, K. R. Electrochemical properties of doped lithium titanate compounds and their performance in lithium rechargeable batteries. *J. Power Sources* **176**, 332–339. https://doi.org/10.1016/j.jpowsour.2007.10.061 (2008).
33. Bauer, D., Roberts, A. J., Matsumi, N. & Darr, J. A. Nano-sized Mo- and Nb-doped TiO_2 as anode materials for high energy and high power hybrid Li-ion capacitors. *Nanotechnology* **28**, 195403. https://doi.org/10.1088/1361-6528/aa69df (2017).
34. Krajewski, M. *et al.* Electrochemical properties of lithium–titanium oxide, modified with Ag–Cu particles, as a negative electrode for lithium-ion batteries. *RSC Adv.* **7**, 52151–52164. https://doi.org/10.1039/C7RA10608D (2017).
35. Baudino, L. *et al.* Stable and reversible lithium storage properties of LiTiOx nanotubes for electrochemical recovery from aqueous solutions. *ChemElectroChem* **9**, e202101652. https://doi.org/10.1002/celc.202101652 (2022).
36. Gao, Q. Optimizing carbon/carbon supercapacitors in aqueous alkali sulfates electrolytes. *J. Energy Chem.* **38**, 219–224. https://doi.org/10.1016/j.jechem.2019.03.037 (2019).
37. Gao, Q., Demarconnay, L., Raymundo-Piñero, E. & Béguin, F. Exploring the large voltage range of carbon/carbon supercapacitors in aqueous lithium sulfate electrolyte. *Energy Environ. Sci.* **5**, 9611–9617. https://doi.org/10.1039/C2EE22284A (2012).
38. Chen, X. *et al.* Production of lithium hydroxide by electrodialysis with bipolar membranes. *Sep. Purif. Technol.* **274**, 119026. https://doi.org/10.1016/j.seppur.2021.119026 (2021).
39. Lu, X. *et al.* Hydrogenated TiO_2 nanotube arrays for supercapacitors. *Nano Lett.* **12**, 1690–1696. https://doi.org/10.1021/nl300173j (2012).
40. Tang, H. *et al.* Enhanced supercapacitive performance on TiO_2@C coaxial nano-rod array through a bio-inspired approach. *Nano Energy* **15**, 75–82. https://doi.org/10.1016/j.nanoen.2015.04.014 (2015).
41. Moon, G. D., Joo, J. B., Dahl, M., Jung, H. & Yin, Y. Nitridation and layered assembly of hollow TiO_2 shells for electrochemical energy storage. *Adv. Funct. Mater.* **24**, 848–856. https://doi.org/10.1002/adfm.201301718 (2014).

Acknowledgements

This research was funded by the National Science Research and Innovation Fund (NSRF) and the Fundamental Fund of Khon Kaen University. Funding was also received from the Research and Graduate Studies of Khon Kaen University. The first author would like to thank Rajamangala University of Technology Rattanakosin, Wang Klai Kangwon Campus, Hua Hin, Prachuap khiri khan, Thailand for partially financial support.

Author contributions

E.S., T.P. and A.K. designed this research. T.P., S.P. and A.K. carried out the experiments. E.S., A.K. T.P. and S.P. analyzed data. E.S., A.K. and T.P. wrote the main manuscript text and prepared all figures. All authors contributed to the scientific discussion and manuscript revisions.

Competing interests

The authors declare no competing interests.

Additional information

Correspondence and requests for materials should be addressed to E.S.

Reprints and permissions information is available at www.nature.com/reprints.

Publisher's note Springer Nature remains neutral with regard to jurisdictional claims in published maps and institutional affiliations.

Open Access This article is licensed under a Creative Commons Attribution 4.0 International License, which permits use, sharing, adaptation, distribution and reproduction in any medium or format, as long as you give appropriate credit to the original author(s) and the source, provide a link to the Creative Commons licence, and indicate if changes were made. The images or other third party material in this article are included in the article's Creative Commons licence, unless indicated otherwise in a credit line to the material. If material is not included in the article's Creative Commons licence and your intended use is not permitted by statutory regulation or exceeds the permitted use, you will need to obtain permission directly from the copyright holder. To view a copy of this licence, visit http://creativecommons.org/licenses/by/4.0/.

© The Author(s) 2024